Journal of Medical Imaging

MedicalImaging.SPIEDigitalLibrary.org

Pixel-based approach to assess contrast-enhanced ultrasound kinetics parameters for differential diagnosis of rheumatoid arthritis

Gaia Rizzo
Bernd Raffeiner
Alessandro Coran
Luca Ciprian
Ugo Fiocco
Costantino Botsios
Roberto Stramare
Enrico Grisan

SPIE.

Pixel-based approach to assess contrast-enhanced ultrasound kinetics parameters for differential diagnosis of rheumatoid arthritis

Gaia Rizzo,[a,*] Bernd Raffeiner,[b] Alessandro Coran,[c] Luca Ciprian,[d] Ugo Fiocco,[c] Costantino Botsios,[c] Roberto Stramare,[c] and Enrico Grisan[a]
[a]University of Padova, Department of Information Engineering, G. Gradenigo 6/A, Padova 35131, Italy
[b]General Hospital of Bolzano, Rheumatology Unit, Via Lorenz Boehler 5, Bolzano 39100, Italy
[c]University of Padova, Department of Medicine, Via Giustiniani 2, Padova 35128, Italy
[d]Nursing Home Giovanni XXIII, Via Giovanni XXIII 7, Monastier di Treviso (TV) 31050, Italy

Abstract. Inflammatory rheumatic diseases are the leading causes of disability and constitute a frequent medical disorder, leading to inability to work, high comorbidity, and increased mortality. The standard for diagnosing and differentiating arthritis is based on clinical examination, laboratory exams, and imaging findings, such as synovitis, bone edema, or joint erosions. Contrast-enhanced ultrasound (CEUS) examination of the small joints is emerging as a sensitive tool for assessing vascularization and disease activity. Quantitative assessment is mostly performed at the region of interest level, where the mean intensity curve is fitted with an exponential function. We showed that using a more physiologically motivated perfusion curve, and by estimating the kinetic parameters separately pixel by pixel, the quantitative information gathered is able to more effectively characterize the different perfusion patterns. In particular, we demonstrated that a random forest classifier based on pixelwise quantification of the kinetic contrast agent perfusion features can discriminate rheumatoid arthritis from different arthritis forms (psoriatic arthritis, spondyloarthritis, and arthritis in connective tissue disease) with an average accuracy of 97%. On the contrary, clinical evaluation (DAS28), semiquantitative CEUS assessment, serological markers, or region-based parameters do not allow such a high diagnostic accuracy. [DOI: 10.1117/1.JMI.2.3.034503]

Keywords: contrast enhanced ultrasound; kinetics analysis; perfusion analysis; parameter estimation; arthritis.

Paper 15071PRR received Apr. 1, 2015; accepted for publication Aug. 13, 2015; published online Sep. 11, 2015.

1 Introduction

Arthritis is a chronic systemic disease whose main characteristic is persistent articular inflammation, which results in joint destruction and loss of function.[1] It is one of the most common causes of disability in industrialized countries, affecting 50 million adults in the US, severely impacting both the individual's wellbeing and the health care system. Among the adults diagnosed with arthritis, 10% of the population suffers from functional limitations attributable to arthritis,[2] such as difficulty in stooping, bending, or kneeling, grasping small objects or carrying weights.[3]

Rheumatoid arthritis (RA) represents the worst outcome among the different forms of arthritis, causing premature mortality, disability, and compromised quality of life.[4] An early diagnosis and effective treatment can avoid the most devastating effects of the disease, but the differential diagnosis is difficult, especially at its onset. In general, the assessment of arthritis activity relies on conventional methods, such as semiquantitative joint assessment by the Disease Activity Score (DAS28) including clinical parameters, serological values and patients' activity assessment. However, joint distribution, clinical manifestations, and radiological appearance may be identical, especially at the beginning of the disease, even if distinct vascularization patterns have been identified in biopsy specimens.[5–7]

From an etiopathological point of view, a crucial event in the pathogenesis of arthritis and RA, in particular, is synovial neovascularization, which is a very early feature of synovial hyperplasia. Over time, inflamed synovial tissue grows irregularly forming invasive pannus tissue, which invades and destroys cartilage and bones. Synovial neovascularization correlates with the activity and aggressiveness of the rheumatoid pannus.[8] Hence, the need for a sensitive imaging technique capable of detecting the grade and extent of intra-articular neovascularization and to characterize the microcirculation patterns of different subtypes of arthritic diseases arises.[9]

A validated method for the estimation of synovitis is dynamic contrast-enhanced magnetic resonance imaging (DCE-MRI) with its proven feasibility to detect signs of synovial inflammation[10] and high sensitivity for early inflammatory and destructive changes in RA joints.[11,12] However, the use of dynamic DCE-MRI to stratify RA versus other types of arthritis led to contrasting results and was shown to be useful to differentiate osteoarthritis from RA[13] but did not have diagnostic utility to distinguish psoriatic arthritis (PSA) from RA.[14,15]

Contrast-enhanced ultrasound (CEUS) imaging of tissue perfusion is based on microbubble echo detection and it allows one

*Address all correspondence to: Gaia Rizzo, E-mail: gaia.rizzo@dei.unipd.it

2329-4302/2015/$25.00 © 2015 SPIE

to noninvasively study the synovial vascularization and local perfusion variations.[16] CEUS has been proven to be a very sensitive tool for assessing arthritis disease activity, at least equivalent to magnetic resonance imaging (with a sensitivity of 95% in detecting knee osteoarthritis[17] and correct differentiation between active and inactive synovitis in 97.3% of joints[18]), but it has several advantages, such as lower cost, portability, shorter examination times, and absence of exposure to radiation or nuclear tracers. However, its capacity in differentiating among different arthritis forms has rarely been evaluated.[19–23]

In clinical practice, CEUS data examination is generally limited to a semiquantitative grading analysis based on International Arthritis Contrast Ultrasound (IACUS) study group guidelines performed by a radiologist, who visually identifies macroscopic areas of vascularization.[16] However, it has been proven that a more complete description of the kinetic perfusion parameters via quantitative approaches can help in the differentiation among various disease forms.[24] Quantification of CEUS data is generally performed at the region of interest (ROI) level, i.e., analyzing the time activity curve (TAC) obtained by averaging all the pixel TACs within a specific user-defined region, via the Qontrast™ software (Esaote S.p.a., Florence, Italy). The ROI level approach is commonly used to quantify CEUS data by using nonlinear estimators since ROI TACs are characterized by a good signal-to-noise ratio. However, a ROI-based approach causes a loss of spatial resolution as it returns only one set of estimated parameters for each region. These regional values are representative of the perfusion behavior within the ROI only if the pixel kinetics is homogenous. If this is not the case, it does not allow one to fully describe the perfusion patterns within the synovia, leading to an impaired description of the perfusion heterogeneity across the joint. On the contrary, pixel level analysis returns one set of estimated parameters for each pixel of the image. This allows one to produce parametric maps with the same spatial resolution as the original CEUS image. The pixel-based analysis is more susceptible to noise and motion artifacts, but it gives the possibility to measure localized perfusion variations.

At variance with other imaging modalities (e.g., PET, MRI) where the transition from region-based to pixel-based quantification has already taken place, there are only few preliminary results on parametric mapping and pixel-based kinetics analysis in CEUS, mostly limited to preclinical and clinical oncology studies,[25–29] and only in one case to classify gliobastoma tissues in humans.[30] In these works, it has been proven that a quantitative pixel-based approach can reveal the heterogeneity of the distribution of the perfusion information[31] and produce the most robust information for tumor diagnostics to separate benign and malignant cases compared to ROI-based analysis.[28]

In this work, we provide a comparison of region-based and pixel-based perfusion kinetic analysis in a dataset of 115 patients affected by either RA or other types of arthritis [PSA and undifferentiated spondyloarthritis (uSPA) and arthritis in connective tissue disease (CTD)] that show similar (i.e., nonsignificantly different) clinical and serological values. We show that by considering the physiological information derived from CEUS images at the pixel level and then by using the pixel-based quantitative features, we can more effectively identify the different perfusion patterns characterizing RA versus other types of disease. We compared the performance of a random forest (RF) classifier trained either on the pixel-level parameters, on the ROI-level parameters, or with the serological values coupled with semiquantitative assessment of CEUS data from the radiologists.

2 Materials and Methods

2.1 *Dataset*

One hundred and fifteen consecutive patients attending the rheumatology outpatient clinic of the University of Padova Hospital between 2008 and 2013 were recruited for the present study.

The cohort included 57 patients with RA (8 males, 49 females; age: 56.3 ± 11.5 years, disease duration: 11.1 ± 8.8 yrs) and 58 patients with nonrheumatoid (non-RA) forms (22 males, 36 females; age: 52.5 ± 12.5 years, disease duration: 10.5 ± 6.8 yrs) (Table 1). Among the non-RA patients, 28 had distal predominant (dpPSA) and 13 polyarticular RA-like PSA, 11 uSPA, and 6 had arthritis in CTD. All patients showed signs of inflammatory finger joint involvement. The patients had to be at least 18 years old and they had to fulfill the criteria for either RA, dpPSA, RA-like SPA, uSPA, or CTD. We excluded patients with major cardiopathy due to potential risks for the use of contrast.

Blood tests were performed, including C-reactive protein (CRP [mg/L]), erythrocyte sedimentation rate (ERS [mm/h]), by the Westergren method], rheumatoid factor (RF [u/mL]), and antibodies against cyclic citrullinated peptides (anti-CCP [U/mL]). These values were used to assess serologic inflammatory activity levels.

The most active joint was chosen for CEUS examination and the clinical diagnosis (as RA, dpPSA, RA-like PSA, Uspa, or CTD) was performed by the rheumatologist based on the clinical patient examination and blood exams. RA was classified following American College of Rheumatology/European League against Rheumatism classification criteria of 2010.[32] Diagnosis of RA-like PSA was established by classification criteria for psoriatic arthritis (CASPAR) and divided into five clinical patterns.[33,34] Classification of uSPA was based on the guidelines presented in Ref. 35. Last, arthritis in CTD was evaluated as in Refs. 36 and 37. The standard and accepted means of defining RA/non-RA arthritis is by use of such classification criteria by the rheumatologist, who performs the clinical diagnosis.[32] This

Table 1 Demographic characteristics in the patient populations. Patient populations are characterized in terms of clinical values (disease duration, age, sex, and therapy) as mean and standard deviation (SD). Rheumatoid arthritis (RA) and non-RA [dpPSA, RA-like psoriatic arthritis (PSA), undifferentiated spondyloarthritis (uSPA), and connective tissue disease (CTD)] are reported separately. Significant differences in the means are evaluated with a one-sided *t*-test (p-value < 0.05).

		Disease duration (years)	Age (years)	Sex (M/F)	Steroid (mg)
RA	Mean	11.1	56.3	8/49	4.70
	SD	8.8	11.5		3.56
Non-RA	Mean	10.5	52.5	22/36	4.13
	SD	6.8	12.5		4.20
t-test		0.70	0.09		0.44
P		n.s.	n.s.		n.s.

Note: n.s., nonsignificant.

was then used as ground truth for the subsequent classification scheme.

2.1.1 *Imaging acquisition*

Each patient's selected joint was examined with CEUS as previously described,[19] using a 7-MHz transducer US device (MyLab25, EsaOte) equipped with contrast tuned imaging (CnTI; Esaote), using a low mechanical index. The mechanical index and acoustic pressure were set at 0.1 and 30 kPa, respectively. The joints were investigated in a sagittal plane from a dorsal view with the hand in a neutral position. The contrast agent for the CEUS analysis was microbubbles filled with sulfur hexafluoride (SonoVue; Bracco International, Princeton, New Jersey). A 4.8-mL bolus of contrast agent was injected into a peripheral vein of the opposite arm, followed by the injection of 20-mL saline solution. The selected joint was scanned in CnTI mode. The recording of the dynamic phases began simultaneously with the bolus injection and continued for 2 min.

Gray-scale US (anatomical B-mode image) was used to gather information on the joint space. The videos obtained were recorded as uncompressed AVI files (11 ± 2 frames/s) and they were digitally stored for subsequent quantitative analysis or manual review.

All patients gave their informed consent to the examination, to the intravenous administration of the contrast agent, and to the participation of the study that was approved by the local institutional ethical committee.

2.1.2 *Clinical assessment*

Synovial contrast enhancement was graded independently by two radiologists using a semiquantitative three-point scale (0 to 2) as recommended by the IACUS study group:[16] grade 0 indicates no visible synovial contrast enhancement, grade 1 indicates a detectable enhancement but less than in the periarticular tissues, and grade 2 indicates an enhancement definitely stronger than in the periarticular structures.[19] Based on the ultrasound appearance and grading, a presumptive diagnosis was proposed by the radiologists for each patient, considering typical histopathological features. In fact, RA is assumed to present a more homogenous synovial enhancement and faster time of contrast appearance due to linear and branching vessel architecture, whereas dpPSA, RA-like SPA, and uSPA have inhomogeneous enhancement both in synovial and perisynovial region representing entheses and capsules, and later contrast appearance due to tortuous, bushy vessels. Arthritis in CTD shows joint effusion without synovitis and neovascularisation.[38] Figure 1 reports an example of CEUS images of RA patients with different IACUS grades.

In addition, the radiologists manually outlined the boundaries of the synovial tissue on the gray-scale US images of each patient, so that the subsequent analysis could be performed on the specific ROI represented by the synovia.

2.2 *Data Preprocessing*

Each examination was composed by an anatomical B-mode image I_{gs}, obtained by the gray-scale US, which allows the identification of the synovial boundaries and the definition of the corresponding synovial mask I_M, and by a video $I^{(t)}_{CEUS}$ imaging the kinetics of the contrast medium. Figure 2 reports a workflow of the acquired data analysis.

In order to provide a reliable analysis, it is imperative that both the US head and the patient's joint do not move during the acquisition and that the anatomical information gathered from I_{gs} can be perfectly superimposed to $I^{(t)}_{CEUS}$: since these conditions are rarely met in clinical settings, it was necessary to register the gray-scale I_{gs} image to each frame of the video with a rigid transformation to correct for possible patient movement and to apply the synovial mask I_M to the CEUS data.

Following the approach presented in Refs. 22 and 24 to register two different acquisitions, we exploited the high reflectivity in both modalities of the superficial tissues of the joint and of the

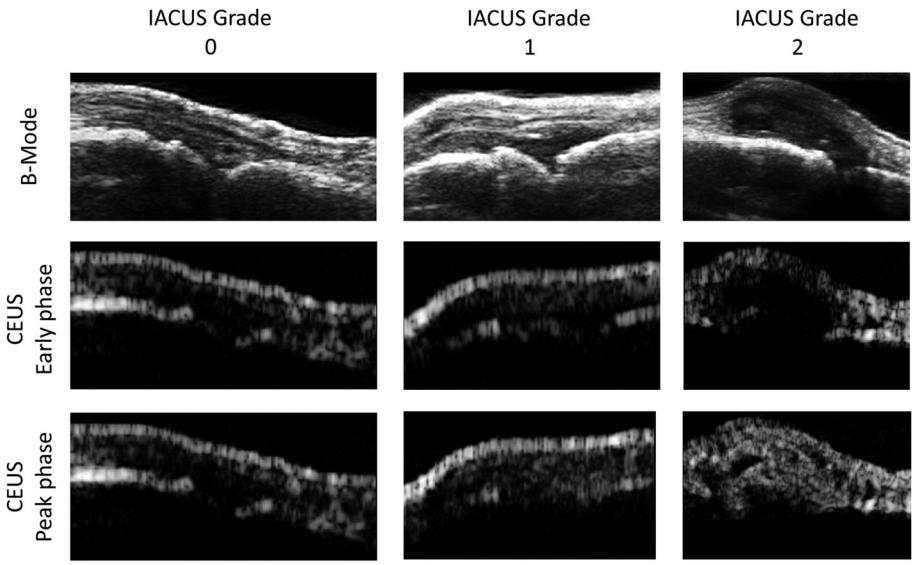

Fig. 1 Contrast-enhanced ultrasound (CEUS) data of rheumatoid arthritis (RA) subjects. The B-mode ultrasound image used as anatomical reference is shown (top panel), together with a CEUS image from an early (middle panel) and late (bottom panel) perfusion phase. Each column represents an RA patient with a different grading (from 0 to 2, left to right).

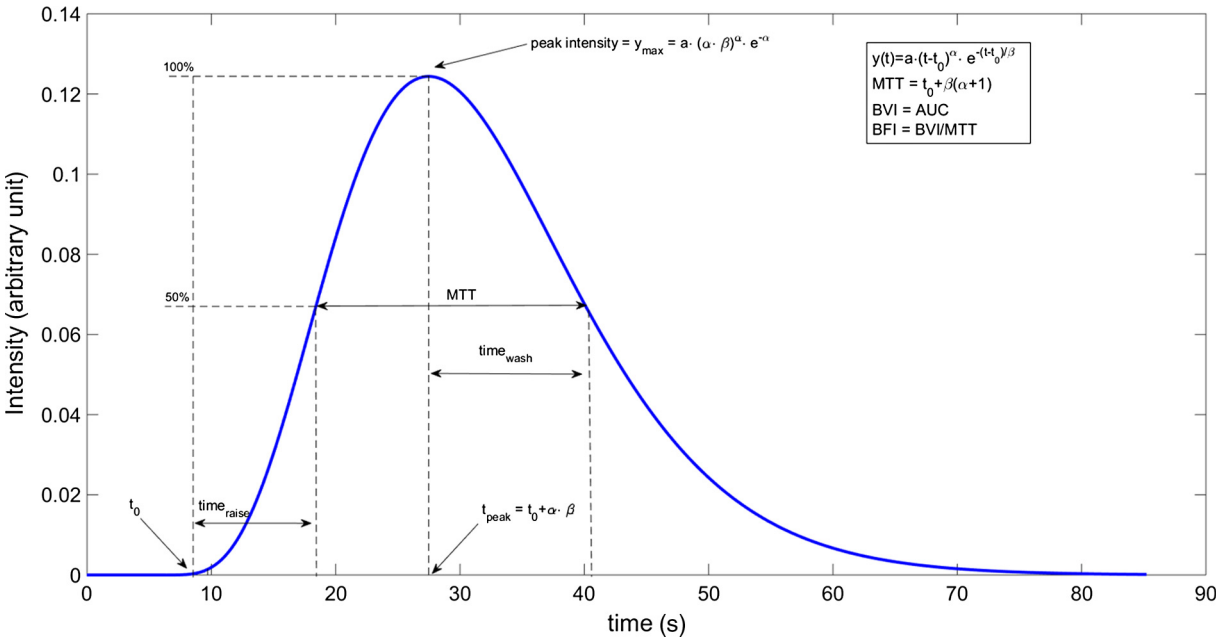

Fig. 2 Profile of a gamma-variate curve. An example of gamma-variate (blue) with the main parameters of interest (t_0, $\text{time}_{\text{raise}}$, $\text{time}_{\text{peak}}$, $\text{time}_{\text{wash}}$, peak value, MTT, blood volume index, blood flow index).

bones. These structures are identified in I_{gs}, in the estimated $I_{\text{baseline}} = E_{t<1.5\ \text{s}}[I^{(t)}_{\text{CEUS}}]$ (i.e., the mean of the harmonic images throughout the first 1.5 s) and on each frame of $I^{(t)}_{\text{CEUS}}$ by segmenting all pixels with intensities greater than the 95% percentile of the image intensities. The displacement between I_{gs} and I_{baseline}, and between each couple of subsequent frames $I^{(i)}_{\text{CEUS}}$ and $I^{(i+1)}_{\text{CEUS}}$, was calculated using the maximum of the phase correlation and was used to map each position on one image into the corresponding position on the other.

Once each patient's CEUS data were registered on the corresponding synovial mask, the perfusion TAC from each pixel within the outlined synovia were extracted ($c_{\text{pixel}\,i}(t)$, for $i = 1, \ldots, N_j$, N_j is the number of pixels in the synovia of the j'th patient, $j = 1, \ldots, M$).

Additionally, the TAC from each pixel within a region surrounding the outlined synovia has been extracted.[19]

2.3 *Model*

The CEUS kinetics $c_{\text{pixel}\,ij}(t)$ was described with a gamma-variate function as in Refs. 22 and 24:

$$c_{\text{gamma}}(t) = \begin{cases} b & t < t_0 \\ b + a \cdot (t - t_0)^{\alpha} \cdot e^{-\frac{t-t_0}{\beta}} & t \geq t_0 \end{cases}, \tag{1}$$

where t_0 represents the contrast arrival time in the ROI, and α and β are two parameters that modulate the raise and washout of the dye from the vascular bed, whereas a accommodates the model for different peak intensity levels and b for different background (or baseline) intensity. An example of the gamma-variate function is reported in Fig. 3.

In order to reduce the computational requirement of identifying the five parameters $[t_0, a, b, \alpha, \beta]$ describing the model of Eq. (1) for each pixel in the synovial regions, we chose to calculate the baseline intensity b as the mean intensity of the first 25 frames corresponding to the first 1 s of the harmonic imaging, usually free from contrast signal. Therefore, the parameter vector to be estimated for each i'th curve is $p_i = [t_0, a, \alpha, \beta]$.

From these parameters, a set of additional model characteristics can be derived, such as the peak value, the time of peak, the raise time, $\text{time}_{\text{raise}}$, and the washout time, $\text{time}_{\text{wash}}$ (computed as the time needed to raise the intensity from the baseline value to half maximum and from the peak value to half maximum, respectively), the blood flow index (BFI) and the blood volume index (BVI), for a total of 10 parameters for each curve (Fig. 3).[39,40]

2.4 *Region of Interest Versus Pixel Level Analysis*

The kinetic estimation analysis was carried out both at the region and pixel levels.

Regarding the region-wise analysis, for each subject there were two different regions of interest, the synovia and the perisynovia, drawn by the radiologists. For each region, the ROI TACs were defined as the average of the pixel perfusion curves within the manually outlined synovial and perisynovial regions. In particular, given the N spatial points $s_i = (x_i, y_i)$ within the mask I_M that show a significant enhancement, considered as the difference between baseline value and peak value larger than a fixed threshold ϑ, the regional perfusion curve $c_{\text{region}}(t)$ is defined as

$$c_{\text{region}}(t) = \frac{1}{N}\sum_i I^{(t)}_{\text{CEUS}}(x_i, y_i) = \frac{1}{N}\sum_i c_{\text{pixel}}(t). \tag{2}$$

The value of the threshold was set to 20% based on previous studies.[19]

The ROI TACs were described with the gamma-variate model of Eq. (1) and the parameters were identified by means of a nonlinear least square fitting, obtaining a set of estimates $\hat{p} = [t_0, a, \alpha, \beta, \text{peak}, \text{time}_{\text{peak}}, \text{time}_{\text{raise}}, \text{time}_{\text{wash}}, \text{BFI}, \text{BVI}]$ for each region.

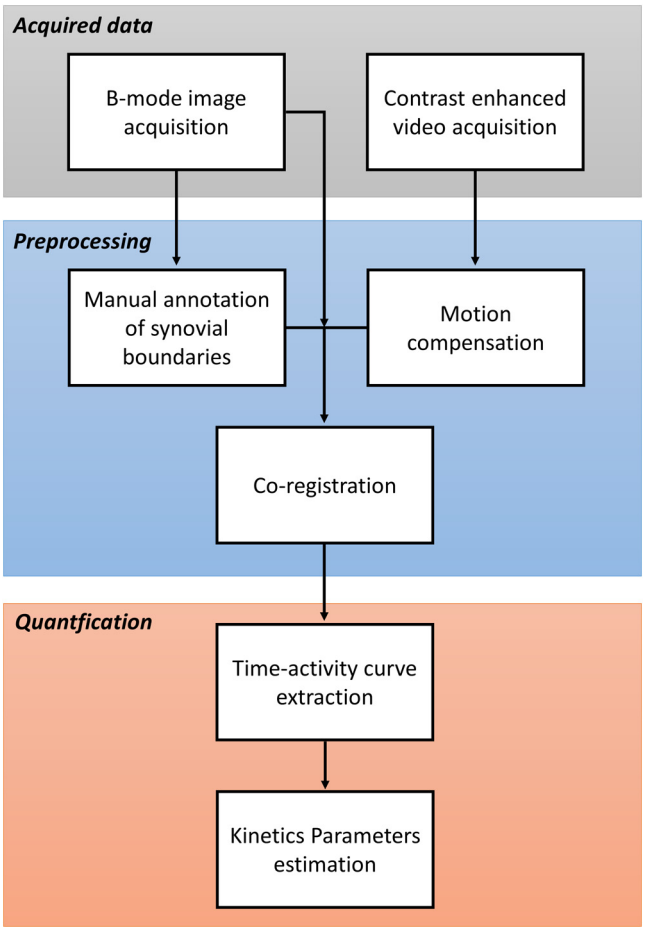

Fig. 3 Data analysis workflow. The first block consists of the acquisition of the B-mode image and of the CEUS video. In the preprocessing phase, the synovia is manually drawn on the B-mode image and the motion correction is performed on the CEUS data, which are then coregistered. In the last block (quantification), the synovial time-activity curves are extracted and the kinetic parameters are estimated both at region and pixel level.

Then for region-based analysis, for each subject, 20 parameters were available (10 for the synovial perfusion and 10 for the perisynovial perfusion) and used as regional features.

On the other hand, when considering a pixel-based approach, each pixel curve c_{pixel} was analyzed independently and described with the same gamma-variate model of Eq. (1). One set of 10 parameters was identified by means of a nonlinear least square fitting for each pixel. We selected as pixel-based features the mean value, the standard deviation, and the 25th and 75th percentiles for each model parameter, so that 80 perfusion features were obtained (40 for the synovial perfusion and 40 for the perisynovial perfusion).

Table 2 reports a summary of the features derived from the quantification analysis of CEUS data.

2.5 *Statistical Analysis*

Demographic and serological population values were tested for statistical significance with a one-sided t-test to assess their mean difference.

CEUS semiquantitative analysis (grade and presumptive diagnosis) and serological values (anti-CCP, RF, DAS28, CRP, and ERS) were also correlated across all subjects in terms of Pearson's correlation (R) in order to evaluate their redundancy.

The performance of the gamma-variate model to fit the data was assessed in terms of visual comparison of the data model fit, the variability of the estimates expressed as their between-subject standard deviation, and the percentage of model failures at the region and pixel levels (failure rate). For the region and pixelwise analysis, failures were defined as estimates with nonphysiological (negative) or unreliable [with a coefficient of variation (CV) >200%] values. The CV returns information about estimate precision. It was calculated from the standard deviation $\text{SD}_{\hat{p}}$ of the estimated parameter $\hat{p}$, as derived by the inverse of the Fisher-information matrix and expressed as a percentage of the estimated parameters as $\text{CV} = \text{SD}_{\hat{p}}/\hat{p} \cdot 100$. Eventual failures at the region and pixel levels were then automatically excluded from the statistical analysis.

Table 2 Quantitative features from regional and pixel level analysis. Summary of the features derived from the quantitative analysis of contrast-enhanced ultrasound (CEUS) data. At region level, there is one feature for each parameter, whereas at pixel level, we derived four features for each parameter (mean, SD, 25th percentile, and 75th percentile).

Parameters	Region based	Pixel based			
t_0	t_{0_ROI}	Mean t_0	SD t_0	25th percentile t_0	75th percentile t_0
a	$a_{\_\text{ROI}}$	Mean a	SD a	25th percentile a	75th percentile a
α	$\alpha_{\_\text{ROI}}$	Mean α	SD α	25th percentile α	75th percentile α
β	$\beta_{\_\text{ROI}}$	Mean β	SD β	25th percentile β	75th percentile β
Peak	$\text{Peak}_{\_\text{ROI}}$	Mean peak	SD peak	25th percentile peak	75th percentile peak
t_p	t_{p_ROI}	Mean t_p	SD t_p	25th percentile t_p	75th percentile t_p
$\text{Time}_{\text{raise}}$	$\text{Time}_{\text{raise\_ROI}}$	Mean $\text{time}_{\text{raise}}$	SD $\text{time}_{\text{raise}}$	25th percentile $\text{time}_{\text{raise}}$	75th percentile $\text{time}_{\text{raise}}$
$\text{Time}_{\text{wash}}$	$\text{Time}_{\text{wash\_ROI}}$	Mean $\text{time}_{\text{wash}}$	SD $\text{time}_{\text{wash}}$	25th percentile $\text{time}_{\text{wash}}$	75th percentile $\text{time}_{\text{wash}}$
BFI	$\text{BFI}_{\_\text{ROI}}$	Mean BFI	SD BFI	25th percentile BFI	75th percentile BFI
BVI	$\text{BVI}_{\_\text{ROI}}$	Mean BVI	SD BVI	25th percentile BVI	75th percentile BVI

Note: BVI, blood volume index; BFI, blood flow index; ROI, region of interest.

In particular, for the pixelwise analysis, we calculated the pixel features for each subject only using the subset of pixels where the model provided reliable estimates (CV <200%).

It is worth noting that nonlinear estimators typically have significant drawbacks when applied pixelwise (i.e., sensitivity to initial estimates, high computational time, nonconvergence in a significant percentage of voxels). However, the results obtained when the estimator converges are characterized by the same properties as the estimator itself, i.e., nonpolarization, consistency, asymptotic normality, and efficiency.[41] For this reason, the pixel estimates that show physiological values and good identifiability can be used for the characterization of CEUS data.

2.6 *Classification*

In order to test the ability of the estimated parameters to characterize different perfusion patterns and to identify the different types of arthritis, we trained a supervised classifier on the estimated parameter statistics (features). We trained an RF classifier,[42,43] an ensemble method that has been proven to be efficient with respect to most single classifiers[43] and to provide competitive performance with support vector machine and boosting. On one side, we used the semiquantitative CEUS and serological values as features; on the other, we used the parameters as features obtained from the quantitative analysis of CEUS examination. In particular, we trained three different classifiers in order to assess the discriminant power of the following sets of features:

a. semiquantitative CEUS grade, presumptive radiological diagnosis and the serological values (including DAS28), i.e., no kinetic analysis;
b. all the 20 ROI-wise kinetic parameters derived as in Qontraxt;
c. pixelwise kinetic features.

Table 3 List of the most relevant 11 pixelwise features. The features' relevance was determined by computing a permutation test on the out-of-bag samples. The most relevant features were selected, discarding the noninformative ones, i.e., those that when included in the classification did not provide any increase in its performance.

Feature	Region	Feature
1	Synovia	mean BFI
2	Synovia	SD peak
3	Synovia	SD BFI
4	Synovia	75th percentile α
5	Synovia	Mean β
6	Synovia	Mean BVI
7	Perisynovia	Mean t_0
8	Perisynovia	Mean peak
9	Synovia	SD α
10	Perisynovia	SD t_0
11	Synovia	Mean peak

In the last case, i.e., pixelwise parameters, in order to reduce the computational complexity and to discard noninformative features, the importance of each feature has been evaluated by computing a permutation test on the out-of-bag samples. By this means, a reduced set of the most relevant 11 features was selected: increasing their number did not provide any increase in the classification performance.

Table 3 reports the reduced set of 11 pixelwise features derived from the permutation test.

In order to assess the statistical power of each set of features for distinguishing different types of arthritis, we used a leave-one-patient-out validation scheme. At each round of the validation, the data of the patient under study were set aside as the test set, while the remaining data were used as the training set. Then the estimation of the overall accuracy, the sensitivity, and the specificity of the classification was reported in the confusion matrix. The classifiers' accuracy was also compared with the assessment performed by the radiologists blinded to the clinical diagnosis.

3 Results

3.1 *Clinical Evaluation*

The mean serological values for the two populations considered (RA Versus non-RA) are reported in Table 4.

Only DAS28, RF, and anti-CCP were statistically different between RA and non-RA patients ($p < 0.05$). Note that the comparison was performed on the between-subject averages of the serological measures and it is not linked to and it does not imply diagnostic accuracy.

Figure 4 reports the autocorrelation analysis between CEUS semiquantitative analysis and serological values: as expected, the CEUS grade and presumptive radiological diagnosis were correlated ($R = 0.6$), indicating the similarity of the information derived from the radiologist examination. In general, serological measures were poorly correlated ($R < 0.4$) with the exception of CRP and ERS ($R = 0.74$), indicating that these values carry the same amount of information. Also, the information derived from CEUS data was additional and uncorrelated with serological markers ($R < 0.35$).

3.2 *Kinetic Analysis*

One of the main advantages of the pixel-based analysis is that it is possible to derive kinetic parameters for each pixel within the synovial area (a so-called parametric map), thus identifying the activity foci and different perfusion patterns. An example of a parametric map of the mean transit time and the time to peak (calculated from the Gamma-variate parameter estimates, as in Ref. 44) is reported in Fig. 5 for a representative RA subject.

All the parametric maps are presented before correction for failures. From Fig. 5, it is plain that the synovial area is characterized by a high degree of heterogeneity: the dye kinetics is not homogenous within the joint and different patterns of functional activity can be observed. The same held when considering other parameters of interest (like t_0, or the time of rise or washout).

The kinetic analysis at the ROI level did not present any failures, the model described the data well, and the parameters were estimated with good precision (on average, each parameter was reliably estimated with a CV smaller than 20%).

Table 4 Mean serological values in the patient populations. Patient populations are characterized in terms of serological values [erythrocyte sedimentation rate (ESR), C-reactive protein (CRP), DAS28, RF, and anti-cyclic citrullinated peptides (CCP)] as mean and SD. RA and non-RA (dpPSA, RA-like PSA, uSPA, and CTD) are reported separately. Significant differences in the means are evaluated with a one-sided *t*-test (p-value < 0.05).

		ESR (mm/h)	CRP (mg/l)	DAS28 (unitless)	RF (u/mL)	Anti-CCP (U/mL)	IACUS grade	Presumptive diagnosis
RA	mean	35.61	17.70	4.50	144.09	126.76	1.52	0.85
	SD	24.27	20.35	1.41	189.79	143.64	0.73	0.36
Non-RA	mean	28.02	14.52	3.80	12.53	19.23	0.73	0.57
	SD	24.82	24.95	1.47	36.20	50.80	0.70	0.50
t-test		0.11	0.46	0.01	0.00	0.00	0.00	0.00
P		n.s.	n.s.	<0.05	<0.05	<0.05	<0.05	<0.05

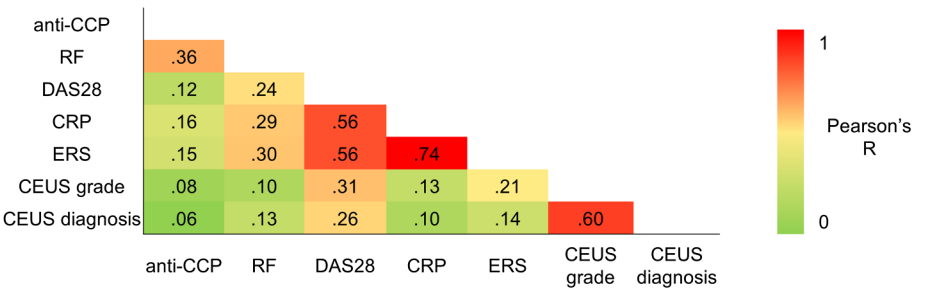

Fig. 4 CEUS semiquantitative analysis and serological values. Correlations of the serological values (anti-cyclic citrullinated peptides, RF, DAS28, C-reactive protein, and ERS) and of the semiquantitative CEUS analysis (grade and presumptive diagnosis) across all subjects are reported in terms of Pearson's correlation (R).

When the gamma variate model was applied at the pixel level, the failure rate increased as expected, and on average $36.5\% \pm 18.5\%$ and $47.1\% \pm 19.2\%$ of pixels had to be eliminated for RA and non-RA patients, respectively. Figure 6 reports an example of the failures' map for two different RA patients, with IACUS grades of 2 and 0, respectively.

Nonetheless, in the remaining set of pixels where the model reliably converged, all parameters were estimated with good precision (on average, all parameters were estimated with a CV smaller than 45%). Interestingly, t_0, which, in general, shows estimates characterized by poor precision[45] was also estimated at the pixel level with a CV of $14.8\% \pm 5.7\%$ and $5.5\% \pm 14.7\%$ for RA and non-RA subjects, respectively.

In Table 5, the between-subject mean and variability of some of the parameters derived from the kinetic analysis at regional and pixel levels (t_0, a, t_{max}, t_{up}, and BFI) are reported separately for RA and non-RA subjects. Pixelwise estimates of the arrival time, the amplitude, and the time rise were higher than those obtained at the region level, albeit not significantly.

3.3 *Classification*

When considering only serological values plus DAS28 and semiquantitative CEUS measures, the RF classifier achieved a specificity of 93%, but a sensitivity of only 64% with an overall accuracy of 84% (Table 6). These results already compared positively with the manual assessment of CEUS examinations alone, performed by the radiologists (blinded to the clinical diagnosis and of the serological values) that showed a high sensitivity (90%), but indeed a low specificity and accuracy (46% and 69%, respectively), and with a classifier based on DAS28 and serum markers alone that showed a sensitivity of 72%, a specificity of 69%, and an overall accuracy of 71%.

Interestingly, the RF classifier trained with the 20 regional kinetic parameters had a worse performance than that using manual semiquantitative assessment, achieving a sensitivity of 60%, a sensitivity of 64%, and an accuracy of 62% (Table 7). This indicates that the regional-based description of the CEUS data is not sufficient to derive a comprehensive description of the heterogeneous kinetic activity in the synovia.

When we considered the pixelwise kinetic analysis, the RF was trained on the reduced set of 11 pixelwise features of Table 3. With this set of features, the classifier achieved a sensitivity of 95%, a specificity of 100%, and an overall accuracy of 97% (Table 8).

4 Discussion

4.1 *Contrast-Enhanced Ultrasound Quantification*

CEUS quantification is generally performed at the ROI level modeling the perfusion curve with a monoexponential

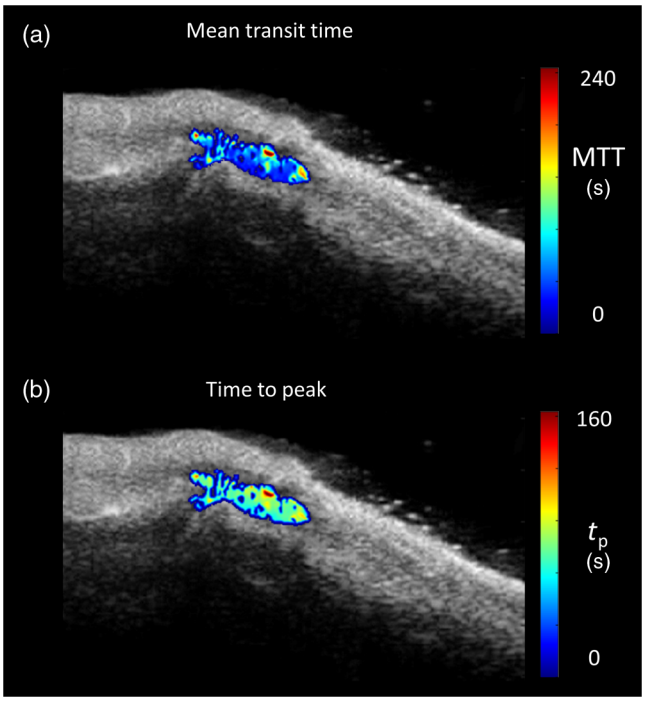

Fig. 5 Parametric maps of quantitative kinetic estimates in a representative RA subject. (a) The mean transit time and (b) the time to peak are reported overlayed on the I_{gs} gray-scaled image. A Gaussian filter (FWHM 2.35 pixels) was used to smooth the images before visualization. Note the heterogeneous distribution of the kinetic parameters within the synovia and the presence of areas in the region of interest with no signal, highlighting the presence or absence of vascularization.

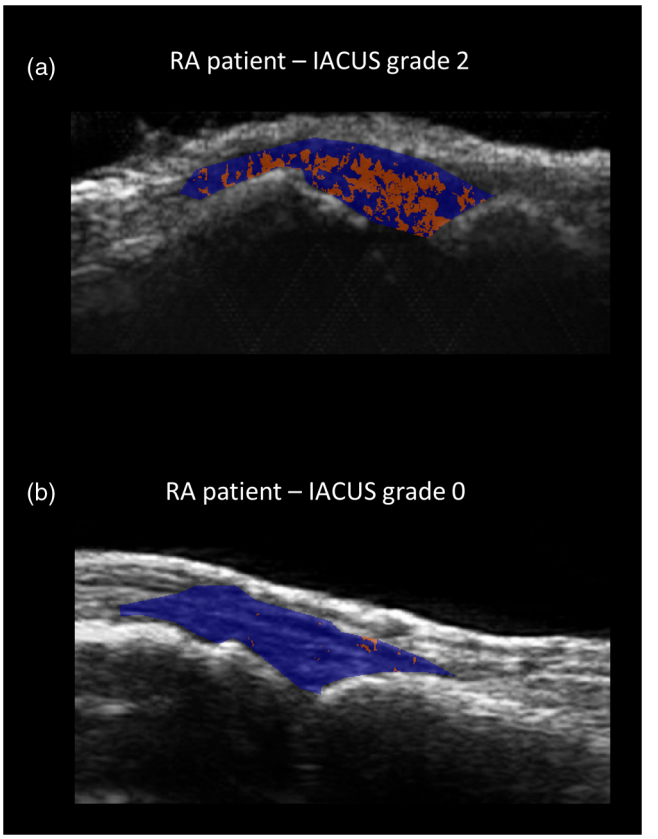

Fig. 6 Map of pixel failures of two RA patients. Parametric maps of pixel failures, which have been eliminated because nonphysiological and/or unreliable (in red) in two different disease conditions overlaid to the correspondent B-mode image. (a) CEUS image of a patient with IACUS grade 2 (35.9% of failures) and (b) CEUS image of a patient with IACUS grade 0 (2.4% of failures).

model,[16,46,47] even if the log-normal or the gamma-variate have been shown to represent a more physiologically motivated model to describe CEUS kinetics.[44,48] In this work, the gamma-variate model was used to describe CEUS kinetics, as previously reported in Refs. 30, 39, and 49. While in many cases, the mono-exponential model can accurately describe the region-based curve, it does not represent the appropriate model for the analysis at the pixel level and in this case, the gamma-variate model (which is a more general and flexible version of the monoexponential model[44]) is to be preferred. In our work, this model properly described the data both at the ROI and pixel levels, in terms of *a posteriori* visual comparison of data fit and of estimate precision (smaller than 20% and 45% at ROI and pixel level, respectively).

The estimator used to solve the model both at the region and pixel levels was the weighted nonlinear least squares. While this represents the method of choice when analyzing data at the region level, the use of nonlinear estimators at the pixel level is difficult and unwieldy because of their computational cost and the high percentage of failures (~40% and ~50% for RA and non-RA patients). Thus, future steps will include the development of more robust and faster estimation algorithms to quantify pixelwise perfusion information in a reasonable computational time.

4.2 *Region of Interest versus Pixel Analysis*

Conventional approaches for quantitative analysis of CEUS data are mainly ROI-based, where a few relatively large regions are manually selected to generate the average curves and used to assess perfusion parameters. In literature, there are also some examples of automatic classification of CEUS data at the region level for the identification of carotid plaques[50] and for the identification of liver lesions[51,52] based on Bayesian and support vector machine classifiers, which are potentially applicable in different anatomical structures.

This approach benefits from a good signal-to-noise ratio, but it is operator dependent and it results in a loss of spatial resolution since it does not allow the quantification of the perfusion information with the same spatial detail as the acquired CEUS data. Also, the average regional TAC is often not representative of the complex heterogeneity of the pixel-based perfusion kinetics in the synovia. Figure 7 reports the perfusion curves obtained by cluster analysis, identifying the principal kinetics present in the synovia of an RA subject. It is plain that a regional-based analysis of CEUS data can only lead to a limited assessment of the parameters of interest, whereas only a pixel-based analysis makes it possible to have a more comprehensive description of the inflamed area.

This is also confirmed by a visual analysis of the parametric maps reported in Fig. 3: different areas of activity are identified in the maps of the mean transit time or the time to peak, and this also holds when considering other parameters of interest (data not shown).

Therefore, we focused our analysis on the pixel level and the results confirmed that only taking into account the full

Table 5 Mean and variability of ROI-wise and pixelwise kinetic parameter estimates. The between-subject mean and variability of the estimates of the arrival time and amplitude of the gamma-variate model (t_0, a) obtained with regional level and pixel level analysis in the synovia are reported separately for RA and non-RA (dpPSA, RA-like PSA, uSPA, and CTD) subjects. Estimates of the derived parameters time of peak (t_{max}), raise time (t_{up}), BFI are also reported for the same region. Significant differences in the means are evaluated with a one-sided t-test (p-value < 0.05).

ROI-wise		a		t_0		α		β		t_{max}		t_{up}		BFI	
RA		0.07	0.06	21.3	12.9	1.0	1.1	33.2	26.4	48.6	32.6	17.6	14.8	0.08	0.05
Non-RA	dpPSA	0.05	0.06	18.6	8.1	0.9	0.9	46.0	31.8	82.3	54.5	23.5	8.7	0.06	0.02
	RA like-PSA	0.02	0.02	11.3	7.7	0.8	0.6	51.0	38.5	45.6	28.0	3.6	11.6	0.05	0.03
	uSPA	0.11	0.10	16.3	11.0	0.8	1.2	27.8	21.9	28.8	13.7	8.7	12.5	0.08	0.08
	CTD	0.03	0.03	10.0	4.6	1.1	1.2	30.4	3.7	82.6	67.1	31.2	46.0	0.07	0.03
	Total	0.06	0.07	15.9	9.1	0.9	0.9	39.8	29.5	63.4	50.3	17.2	22.4	0.06	0.04
t-test		0.27		0.005		0.96		0.06		0.05		0.19		0.08	
p-value		n.s.		<0.05		n.s.		n.s.		<0.05		n.s.		n.s.	
Pixelwise		a		t_0		α		β		t_{max}		t_{up}		BFI	
RA		0.11	0.11	26.4	16.2	0.8	0.9	32.8	27.6	45.1	18.9	21.3	13	0.08	0.05
Non-RA	dpPSA	0.10	0.13	24.8	11.8	0.8	1.1	32.4	29.4	57.4	20.9	26.7	17.1	0.06	0.03
	RA like-PSA	0.05	0.07	19.5	11.2	1.0	1.3	36.3	30.7	41.5	19.7	15.3	9.8	0.07	0.04
	uSPA	0.20	0.12	19.7	10.9	0.5	0.6	41.7	29.9	31.0	13.6	13.1	12.0	0.08	0.08
	CTD	0.02	0.06	26.2	13.8	1.9	1.4	42.3	35.0	98.2	21.0	52.2	27.0	0.12	0.05
	total	0.10	0.11	24.5	15.6	0.9	1.1	33.4	28.6	50.4	24.8	22.8	17.8	0.07	0.05
t-test		0.51		0.31		0.003		0.52		0.31		0.09		0.02	
p-value		n.s.		n.s.		<0.05		n.s.		n.s.		n.s.		<0.05	

Table 6 Confusion matrix for the random forest classification using semiquantitative CEUS and serological values. Patient populations are divided into RA and non-RA (dpPSA, RA-like PSA, uSPA and CTD). Semiquantitative CEUS radiological analysis (CEUS grade and diagnosis) and serological values (ESR, CRP, DAS28, RF, anti-CCP, plus DAS28) were used for the classification. For each of the two classes, positive and negative predicted values (PPV and NPV, respectively), specificity and sensitivity are reported. The accuracy is reported in bold values at bottom right.

		Clinical diagnosis						
		RA	dpPSA	RA-like PSA	uSPA	CTD		
RF classification using CEUS radiological diagnosis	RA	21	0	5	0	0	**0.81**	**PPV**
	dpPSA RA like-PSA uSPA CTD	12		67			**0.80**	**NPV**
		0.64		**0.93**			**0.84**	
		Sensitivity		**Specificity**				

Table 7 Confusion matrix for the random forest classification using with CEUS ROI-wise kinetic parameters. Patient populations are divided into RA and non-RA (dpPSA, RA-like PSA, uSPA, and CTD). The classification was performed based on 16 regional kinetic parameters computed as in Qontraxt. For each of the two classes, PPV and NPV, respectively, specificity and sensitivity are reported. The accuracy is reported in bold values at bottom right.

		Clinical diagnosis						
		RA	dpPSA	RA-like PSA	uSPA	CTS		
RF classification using ROI-wise CEUS	RA	34	10	9	2	0	**0.62**	**PPV**
	dpPSA RA like-PSA Uspa CTD	23		37			**0.80**	**NPV**
		0.60 **Sensitivity**		**0.64** **Specificity**			**0.62**	

Table 8 Confusion matrix for the random forest classification using with CEUS pixelwise kinetic parameters. Patient populations are divided into RA and non-RA (PSA, dpPSA, simRA, uSPA, and CTD). The classification was performed based on the 11 kinetic features derived from the pixelwise analysis of all the subjects. For each of the two classes, PPV and NPV, respectively, specificity and sensitivity are reported. The accuracy is reported in bold values at bottom right.

		Clinical diagnosis						
		RA	dpPSA	RA-like PSA	uSPA	CTD		
RF classification using pixelwise CEUS	RA	54	0	0	0	0	**1.00**	**PPV**
	dpPSA RA like-PSA uSPA CTD	3		58			**0.80**	**NPV**
		0.95 **Sensitivity**		**1.00** **Specificity**			**0.97**	

distribution of the kinetic parameters in the area of interest, it is possible to accurately differentiate RA and non-RA patients. We want to stress that we do not propose any novel technique for image or kinetic analysis, but we provide new insights on what can be obtained, in term of disease and patient characterization, with a different quantification approach from that currently used in the clinical practice. In particular, the main novelty of the work is in the level of resolution chosen for the analysis (pixel-based and not ROI-based).

In fact, when the ROI-wise parameters were used to train the classifier, its performance was even worse than that obtained when considering only serological values and semi-quantitative measures. On the contrary, when using kinetic parameters obtained at the pixel level to train the classifier, it was possible to differentiate between RA and non-RA patients with a sensitivity of 95%, a specificity of 100%, and an overall accuracy of 97%. These results point out how a regional-based analysis is not appropriate for the assessment of CEUS data to distinguish among different forms of arthritis. Also, we demonstrated the possibility of using perfusion parameters to obtain quantitative and reliable information on the subtle differences in perfusion patterns, even when there are limited clinical differences. It is important to highlight that the method proposed here is independent from any serological measures and from the evaluation of the CEUS images performed by the radiologists. This approach, therefore, removes the need for serum markers and visual evaluation of CEUS images from the radiologists, as it greatly improves the classification results obtained when only serological measures, presumptive diagnosis, and grading are used.

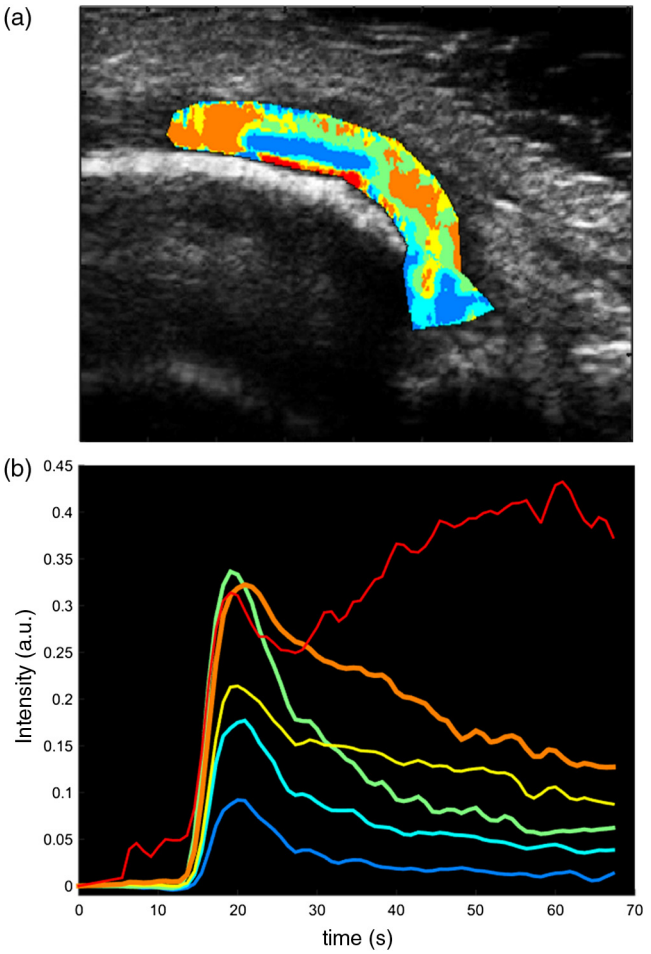

Fig. 7 Heterogeneity of kinetic patterns in a representative RA-like psoriatic arthritis (PSA) subject. (a) The cluster results show the presence of heterogeneous perfusion kinetics within the same synovial area in a RA-like PSA subject. Cluster kinetics were derived with *k*-means partitioning method[53] (Euclidean distance, six clusters). (b) The corresponding time activity curves are reported for each cluster. All the centroids are significantly different (two-sided rank sum test, $p < 0.05$).

5 Conclusions

We compared region-based and pixel-based quantitative analysis of contrast kinetics in CEUS, for the assessment of perfusion patterns in different types of arthritis. While regional analysis failed in characterizing perfusion variability, pixel-based perfusion markers provided a larger number of kinetic features, the localization of perfusion patterns from the parametric maps, and the evidence of kinetics differences in different arthritis. Moreover, pixelwise analysis provided a high accuracy in discriminating RA from non-RA arthritis, showing the ability of CEUS in the identification of distinctive vascularization patterns, even when no or mild clinical differences are present.

Acknowledgments

This work has been partially funded by the University of Padova Grant Nos. 60A11-8427 and 60A11-7979.

References

1. J. M. Dayer and E. Choy, "Therapeutic targets in rheumatoid arthritis: the interleukin-6 receptor," *Rheumatology* **49**(1), 15–24 (2010).
2. J. M. Hootman and C. G. Helmick, "Projections of US prevalence of arthritis and associated activity limitations," *Arthritis Rheumatol.* **54**(1), 226–229 (2006).
3. K. A. Theis et al., "Social participation restriction among US adults with arthritis: a population-based study using the international classification of functioning, disability and health," *Arthritis Care Res.* **65**(7), 1059–1069 (2013).
4. P. M. Brooks, "The burden of musculoskeletal disease—a global perspective," *Clin. Rheumatol.* **25**(6), 778–781 (2006).
5. J. S. Smolen et al., "Treating rheumatoid arthritis to target: recommendations of an international task force," *Ann. Rheumatol. Dis.* **69**(4), 631–637 (2010).
6. U. Fiocco et al., "Vascular changes in psoriatic knee joint synovitis," *J. Rheum.* **28**(11), 2480–2486 (2001).
7. G. Salvador et al., "Synovial vascular patterns and angiogenic factors expression in synovial tissue and serum of patients with rheumatoid arthritis," *Rheumatology* **45**(8), 966–971 (2006).
8. S. Hirohata and J. Sakakibara, "Angioneogenesis as a possible elusive triggering factor in rheumatoid arthritis," *Lancet* **353**(9161), 1331 (1999).
9. D. F. Ten Cate et al., "Role of ultrasonography in diagnosing early rheumatoid arthritis and remission of rheumatoid arthritis—a systematic review of the literature," *Arthritis Res. Ther.* **15**(1), R4 (2013).
10. M. Østergaard et al., "Quantification of synovistis by MRI: correlation between dynamic and static gadolinium-enhanced magnetic resonance imaging and microscopic and macroscopic signs of synovial inflammation," *Magn. Reson. Imaging* **16**(7), 743–754 (1998).
11. M. Ostergaard, B. Ejbjerg, and M. Szkudlarek, "Imaging in early rheumatoid arthritis: roles of magnetic resonance imaging, ultrasonography, conventional radiography and computed tomography," *Best Pract. Res. Clin. Rheumatol.* **19**(1), 91–116 (2005).
12. S. Orguc et al., "Comparison of OMERACT-RAMRIS scores and computer-aided dynamic magnetic resonance imaging findings of hand and wrist as a measure of activity in rheumatoid arthritis," *Rheumatol. Int.* **33**(7), 1837–1844 (2013).
13. E. Kirkhus et al., "Contrast-enhanced dynamic magnetic resonance imaging of finger joints in osteoarthritis and rheumatoid arthritis: an analysis based on pharmacokinetic modeling," *Acta Radiol.* **47**(8), 845–851 (2006).
14. H. Marzo-Ortega et al., "Magnetic resonance imaging in the assessment of metacarpophalangeal joint disease in early psoriatic and rheumatoid arthritis," *Scand. J. Rheumatol.* **38**(2), 79–83 (2009).
15. M. A. Cimmino et al., "Dynamic magnetic resonance of the wrist in psoriatic arthritis reveals imaging patterns similar to those of rheumatoid arthritis," *Arthritis Res. Ther.* **7**(4), R725–731 (2005).
16. A. Klauser et al., "Contrast enhanced gray-scale sonography in assessment of joint vascularity in rheumatoid arthritis: results from the IACUS study group," *Eur. Radiol.* **15**(12), 2404–2410 (2005).
17. I. H. Song et al., "Knee osteoarthritis. Efficacy of a new method of contrast-enhanced musculoskeletal ultrasonography in detection of synovitis in patients with knee osteoarthritis in comparison with magnetic resonance imaging," *Ann. Rheum. Dis.* **67**(1), 19–25 (2008).
18. T. De Zordo et al., "Value of contrast-enhanced ultrasound in rheumatoid arthritis," *Eur. J. Radiol.* **64**(2), 222–230 (2007).
19. R. Stramare et al., "Evaluation of finger joint synovial vascularity in patients with rheumatoid arthritis using contrast-enhanced ultrasound with water immersion and a stabilized probe," *J. Clin. Ultrasound* **40**(3), 147–154 (2012).
20. U. Fiocco et al., "Vascular perfusion kinetics by contrast-enhanced ultrasound are related to synovial microvascularity in the joints of psoriatic arthritis," *Clin. Rheumatol.* (2015).
21. E. Grisan et al., "Toward early detection and differentiation of arthritic diseases: quantification of haemodynamics changes in small joints," in *World Congress on Medical Physics and Biomedical Engineering, September 7–12, 2009, Munich, Germany*, O. Dössel and W. Schlegel, Eds., pp. 470–473, Springer, Berlin Heidelberg (2009).
22. E. Grisan et al., "Dynamic automated synovial imaging (DASI) for differential diagnosis of rheumatoid arthritis," *Proc. SPIE* **9035**, 903514 (2014).
23. G. Rizzo et al., "Data-driven learning to detect characteristic kinetics in ultrasound images of arthritis," in *3rd MICCAI 2014 Workshop on Clinical Image-based Procedures: Translational Research in*

Medical Imaging, M. G. Linguraru et al., pp. 17–24, Springer International Publishing, Boston (2014).
24. E. Grisan et al., "A comparison of region-based and pixel-based CEUS kinetics parameters in the assessment of arthritis," *Proc. SPIE* **9040**, 90400F (2014).
25. R. E. Pollard et al., "Motion corrected cadence CPS ultrasound for quantifying response to vasoactive drugs in a rat kidney model," *Urology* **74**(3), 675–681 (2009).
26. D. B. Ellegala et al., "Imaging tumor angiogenesis with contrast ultrasound and microbubbles targeted to alpha(v)beta3," *Circulation* **108**(3), 336–341 (2003).
27. N. G. Rognin et al., "Parametric imaging for characterizing focal liver lesions in contrast-enhanced ultrasound," *IEEE Trans. Ultrasonics Ferroelectr. Freq. Control* **57**(11), 2503–2511 (2010).
28. C. N. Ta et al., "Automating tumor classification with pixel-by-pixel contrast-enhanced ultrasound perfusion kinetics," *J. Vac. Sci. Technol. B* **30**(2), 02C103 (2012).
29. K. Mahéo et al., "Non-invasive quantification of tumor vascular architecture during docetaxel-chemotherapy," *Breast Cancer Res. Treat.* **134**(3), 1013–1025 (2012).
30. K. Ritschel, I. Pechlivanis, and S. Winter, "Brain tumor classification on intraoperative contrast-enhanced ultrasound," *Int. J. Comp. Assist. Radiol. Surg.* **10**(5), 531–540 (2015).
31. G. Xiaolin et al., "Parametric perfusion imaging using contrast enhanced ultrasound with bolus administration of contrast agents," in *IEEE-EMBS Int. Conf. on Biomedical and Health Informatics*, pp. 663–666 (2012).
32. D. Aletaha et al., "2010 Rheumatoid arthritis classification criteria: an American College of Rheumatology/European League Against Rheumatism collaborative initiative," *Ann. Rheum. Dis.* **69**(9), 1580–1588 (2010).
33. W. Taylor et al., "Classification criteria for psoriatic arthritis: development of new criteria from a large international study," *Arthritis Rheumat.* **54**(8), 2665–2673 (2006).
34. S. M. Jones et al., "Psoriatic arthritis: outcome of disease subsets and relationship of joint disease to nail and skin disease," *Br. J. Rheumatol.* **33**(9), 834–839 (1994).
35. M. Rudwaleit et al., "The Assessment of SpondyloArthritis International Society classification criteria for peripheral spondyloarthritis and for spondyloarthritis in general," *Ann. Rheum. Dis.* **70**(1), 25–31 (2011).
36. R. P. Kimberly, "Connective tissue diseases," in *Primer on the Rheumatic Diseases*, J. H. Klippel, Ed., pp. 325–325, Springer Science & Business Media, Georgia (2001).
37. M. Mosca et al., "The diagnosis and classification of undifferentiated connective tissue diseases," *J. Autoimmun.* **48–49**, 50–52 (2014).
38. R. J. Reece et al., "Distinct vascular patterns of early synovitis in psoriatic, reactive, and rheumatoid arthritis," *Arthritis Rheumat.* **42**(7), 1481–1484 (1999).
39. T. T. Rissanen et al., "High-resolution ultrasound perfusion imaging of therapeutic angiogenesis," *J. Am. Col. Cardiol.* **1**(1), 83–91 (2008).
40. P. Angelelli et al., "Interactive visual analysis of contrast-enhanced ultrasound data based on small neighborhood statistics," *Comp. Graph.* **35**(2), 218–226 (2011).
41. C. Cobelli and E. R. Carson, *Introduction to Modeling in Physiology and Medicine*, Academic Press, San Diego (2008).
42. Y. Amit and D. Geman, "Shape quantization and recognition with randomized trees," *Neural Comput.* **9**(7), 1545–1588 (1997).
43. L. Breiman, "Random forests," *Mach. Learn.* **45**(1), 5–32 (2001).
44. C. Strouthos et al., "Indicator dilution models for the quantification of microvascular blood flow with bolus administration of ultrasound contrast agents," *IEEE Trans. Ultrasonics Ferroelectr. Freq. Control* **57**(6), 1296–1310 (2010).
45. M. Tonietto et al., "Improved models for plasma radiometabolite correction and their impact on kinetic quantification in PET studies," *J. Cereb. Blood Flow Metab.* **35**(9), 1462–1469 (2015).
46. A. S. Klauser et al., "Contrast-enhanced ultrasonography for the detection of joint vascularity in arthritis-subjective grading versus computer-aided objective quantification," *Ultraschall Med.* **32**(Suppl. 02), E31–E37 (2011).
47. H. Platzgummer et al., "Quantification of synovitis in rheumatoid arthritis: do we really need quantitative measurement of contrast-enhanced ultrasound?," *Eur. J. Radiol.* **71**(2), 237–241 (2009).
48. L. Ostergaard et al., "High resolution measurement of cerebral blood flow using intravascular tracer bolus passages. Part I: mathematical approach and statistical analysis," *Magn. Reson. Med.* **36**(5), 715–725 (1996).
49. M. Yu et al., "Clinical application of contrast-enhanced ultrasonography in diagnosis of superficial lymphadenopathy," *J. Ultrasound Med.* **29**(5), 735–740 (2010).
50. O. Hjelmgren et al., "Identification of vascularised carotid plaques using a standardised and reproducible technique to measure ultrasound contrast uptake," *Eur. J. Vasc. Endovasc. Surg.* **46**(1), 21–28 (2013).
51. S. Bakas et al., "Automatic identification and localisation of potential malignancies in contrast-enhanced ultrasound liver scans using spatio-temporal features," in *6th Int. Workshop, ABDI 2014 Held in Conjunction with MICCAI*, H. Yoshida, J. J. Näppi, and S. Saini, Eds., pp. 13–22, Springer International Publishing Switzerland, Cambridge, Massachusetts (2014).
52. I. Gatos et al., "A new automated quantification algorithm for the detection and evaluation of focal liver lesions with contrast-enhanced ultrasound," *Med. Phys.* **42**(7), 3948 (2015).
53. J. MacQueen, "Some methods for classification and analysis of multivariate observations," in *Proc. of Fifth Berkeley Symposium on Mathematical Statistics and Probability*, Statistics, Vol. 1, pp. 281–297 (1967).

Gaia Rizzo received his PhD degree in bioengineering from the University of Padova in 2012. Since March 2014 she is a senior postdoc at the Department of Information Engineering, University of Padova. She was visiting researcher at the Imperial College of London and the King's College London (2008-2014). Her research activity focuses on the quantification of PET images, integration of genomic and neuroimaging data and development of methods for the kinetic analysis of ultrasound images.

Ugo Fiocco is specialized in rheumatology, allergology, and immunology. He is an assistant professor of internal medicine, University of Padova from 1976 to 1980. He is teaching in the University of Padova: School of Rheumatology; Allergology and Immunology and Physical Medicine and Rehabilitation. He is the head of the "Diagnostic and Intraarticular-Arthroscopic Therapy" unit of the Multidisciplinary Day Surgery Department, Padova University Hospital. He is the member of Italian Society of Rheumatology and American College of Rheumatology. His scientific publications are on pathology, diagnostic imaging, and immunotherapy of rheumatic diseases.

Costantino Botsios is graduated in medicine and surgery at the University of Padova, Italy. He is a specialist in rheumatology and received his PhD in clinical and experimental rheumatology and gerontology at the University of Padova. He is a specialist dedicated to biological therapy in the Rheumatology Unit, Department of Medicine, University of Padova. His field of interest is the treatment of rheumatoid arthritis and spondyloarthritis with biological drugs. He is the member of Italian Society of Rheumatology.

Enrico Grisan received his PhD in bioengineering jointly from the University of Padova and City University London in 2005. Currently, he is assistant professor in the Department of Information Engineering, University of Padova. His main interests are the processing and analysis of biomedical images, in particular in the field of retinal imaging, optical endoscopy and confocal microendoscopy, ultrasound, and MRI.

Biographies for the other authors are not available.